Energy- and angle-resolved ionization of H_2^+ interacting with xuv subfemtosecond laser pulses

R. E. F. Silva,[1,*] F. Catoire,[2,†] P. Rivière,[1] T. Niederhausen,[1] H. Bachau,[2] and F. Martín[1,3,4,‡]

[1]*Departamento de Química, Universidad Autónoma de Madrid, E-28049 Madrid, Spain*

[2]*Centre des Lasers Intenses et Applications CNRS-CEA-Université de Bordeaux, 351 Cours de la Libération, F-33405 Talence, France*

[3]*Instituto Madrileño de Estudios Avanzados en Nanociencia, Cantoblanco, E-28049 Madrid, Spain*

[4]*Condensed Matter Physics Center, Universidad Autónoma de Madrid, E-28049 Madrid, Spain*

(Received 15 May 2015; published 29 July 2015)

We present an extension of the resolvent operator method to extract fully differential ionization probabilities resulting from the interaction of ultrashort laser pulses with H_2^+ by including all electronic and vibrational (dissociative) degrees of freedom. The wave function from which ionization probabilities are extracted is obtained by solving the time-dependent Schrödinger equation in a grid for the case of H_2^+ oriented parallel to the polarization direction of the field. The performance of the method is illustrated by using pulses in the xuv domain. Correlated kinetic-energy (CKE) and correlated angular and nuclear kinetic-energy (CAK_N) spectra have been evaluated and used to analyze the underlying mechanisms of the photoionization process. In particular, for pulses with a central frequency $\omega = 0.8$ a.u., which is smaller than the vertical ionization potential of H_2^+, we show the opening of the one-photon ionization channel by decreasing the pulse duration down to less than 1 fs. An analysis of the CKE and CAK_N spectra allows us to visualize individual contributions from one- and two-photon ionization processes, as well as to study the variation of these contributions with pulse duration. The latter information is difficult to extract when only the kinetic energy release (KER) spectrum is measured. This points out the importance of performing multiple-coincidence measurements for better elucidation of competing ionization mechanisms, such as those arising when ultrashort pulses are used.

DOI: 10.1103/PhysRevA.92.013426 PACS number(s): 33.20.Xx, 33.80.Rv, 33.60.+q

I. INTRODUCTION

The development of intense xuv sources through free-electron lasers (FEL) [1,2] and high-order-harmonic generation (HHG) [3–5] in the femtosecond (fs) and sub-fs domains provides a unique tool to investigate laser-matter interaction at ultrashort-time durations. Some fundamental processes, like the photoionization of atoms or molecules, are now being reinvestigated to get a better understanding of their dynamics at ultrashort time. For example, in the case of atoms, delays in photoionization have been measured [6–8], initiating tremendous activity in the calculation and measurement of ionization delays. In molecules, real-time imaging techniques have been applied to pump-probe experiments, and it is now possible to follow in time the dissociative ionization of simple molecules, such as H_2 [9–12], or ultrafast charge migration in biomolecules [13]. Most of these studies rely on pump-probe schemes with an xuv pump pulse and an infrared probe pulse. The difficulty of using an ir probe is that it influences the outcome of the experiment, even if a rather low intensity (a few terawatts) is used. In the case of molecules, the ir field may distort the molecular surface potential and, consequently, affect the molecular dynamics. The other difficulty is that the ir fields may induce nonlinear effects, leading to complex dynamics that is usually difficult to interpret. Recent works [14–17] have succeeded in implementing pump-probe schemes in which only xuv fs pulses are used. These schemes are paving the way for us to explore electronic dynamics with almost no distortion of the molecular surface potential [18] (due to the short wavelength) and involve a small number of absorbed photons, typically one or two per pulse.

In addition to the important progress achieved in the generation of xuv pulses of increasingly higher intensity and shorter duration, experimental schemes making use of such pulses are usually combined with sophisticated detection techniques, such as the so-called cold-target recoil-ion momentum spectroscopy technique (COLTRIMS) [19], which allows for the detection of ionic fragments and electrons in coincidence. An example has been recently reported in [20], where the electron angular distributions were measured in coincidence with the proton kinetic-energy release (KER) in H_2^+ multiphoton ionization induced by ultrashort pulses.

In this context, it is of interest to reexamine elementary and fundamental processes, such as those induced by fs and sub-fs xuv fields in molecules. In particular, it is important to evaluate electron angular and ion kinetic-energy distributions and the correlations between them. The ideal system to do so is H_2^+, for which one can expect to obtain a nearly exact theoretical description, i.e., free from errors resulting from approximations commonly used in more complex molecular systems. Furthermore, in H_2^+, nuclear motion typically occurs on the few-fs time scale, so that the dynamics of dissociative ionization, which is the accessible process in multiple-coincidence measurements, is expected to result from the coupled motion of electrons and nuclei and to be sensitive to the variation of the pulse duration around 1 fs.

In this work, we consider photon energies in the range of 0.4–0.8 a.u. (i.e., 11–22 eV, currently produced in FEL and HHG facilities), for which photoionization of H_2^+ requires the absorption of, at most, two photons. We solve the time-dependent Schrödinger equation (TDSE), which has been shown to be a very efficient method to extract the relevant physical quantities for this system when ultrashort pulses are

*rui.silva@uam.es
†catoire@celia.u-bordeaux1.fr
‡fernando.martin@uam.es

involved [21–23]. In previous works, both the electronic and vibrational (dissociative) motions were taken into account in full dimensionality by using an L^2 spectral method within the adiabatic approximation [22–24]. This approximation has been successfully used for H_2^+ in several contexts [22,23], but it is expected to fail when, e.g., the electron is emitted with a velocity comparable to that of the nuclei or when the dynamics proceeds through avoided crossings between potential-energy curves. To go beyond the adiabatic approximation, one has to incorporate nonadiabatic couplings, which require cumbersome developments. Alternatively, the TDSE can be numerically solved on a discretized spatial grid [25], which has the advantage that going beyond the adiabatic approximation is straightforward. However, unlike spectral methods, extraction of the observables at the end of the pulse is not a trivial task.

Recently, we have proposed the use of the resolvent-operator method (ROM), initially designed for atomic systems [26,27], to calculate correlated kinetic-energy (CKE) spectra (in electronic and nuclear energies) [28,29] of a low-dimensionality (1+1)D H_2^+ molecule irradiated by xuv and ir fields [the (1+1)D notation indicates one degree of freedom for the electronic motion and another one for nuclear motion]. Here we extend this method (i) to treat the electronic motion in full dimensionality [three-dimensional (3D)] and (ii) to extract photoelectron angular distributions. Therefore, in addition to CKE spectra, we evaluate correlated angular and nuclear kinetic-energy spectra, referred to as CAK_N spectra. We show that, at a given photon energy, the total KER strongly depends on the pulse duration, which is the signature of multiphoton processes of different orders contributing to the same ionization signal. We also show that correlated spectra, in particular the CAK_N, allows one to separate the contribution from the different channels in a very simple way, which provides new insight on the photoionization of H_2^+ not accounted for in previous work.

Atomic units are used throughout unless otherwise stated.

II. THEORETICAL FRAMEWORK

A. Full-dimensional model for H_2^+

The full nonrelativistic field-free Hamiltonian for the H_2^+ one-electron homonuclear diatomic molecule in the body-fixed reference frame after separating the dynamics of the center of mass is [30]

$$\hat{H}_0 = -\frac{1}{2M}\nabla^2_{\mathbf{R}} - \frac{1}{2\mu_e}\nabla^2_{\mathbf{r}} + V_C, \tag{1}$$

where $M = M_p/2$ is the reduced mass of the nuclei and M_p is the mass of the proton. In the present work we set $M = 918.076$, and $\mu_e = 2M_p/(2M_p + 1)$ is the reduced mass of the electron. V_C is the sum of all Coulomb potential terms. The internuclear coordinate is represented by $\mathbf{R}$, and the electronic coordinates are represented by $\mathbf{r}$. Neglecting all rotational effects fixes the orientation of the internuclear axis. Following the work of [31], we will use cylindrical coordinates (ρ, z, ϕ, R) (see Fig. 1), where ρ, z, and ϕ define the position of the electron and R is the internuclear distance. In these coordinates, the Hamiltonian is written

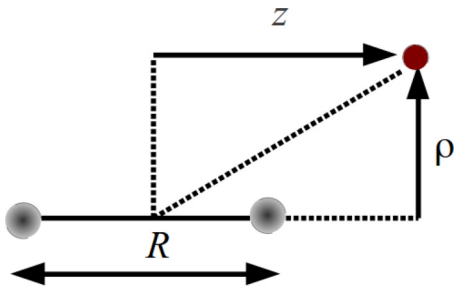

FIG. 1. (Color online) Coordinate system used to describe the H_2^+ system in cylindrical coordinates. The laser pulse is aligned along the internuclear axis.

$$\hat{H}_0 = -\frac{1}{2M}\frac{\partial^2}{\partial R^2} + V_C - \frac{1}{2\mu_e}\left(\frac{\partial^2}{\partial\rho^2} + \frac{1}{\rho}\frac{\partial}{\partial\rho} + \frac{\partial^2}{\partial z^2} + \frac{1}{\rho^2}\frac{\partial^2}{\partial\phi^2}\right), \tag{2}$$

$$V_C = \frac{1}{R} - \frac{1}{\sqrt{\rho^2 + (z + R/2)^2}} - \frac{1}{\sqrt{\rho^2 + (z - R/2)^2}}. \tag{3}$$

We will study laser fields that are polarized along the z axis, and we start from states with $m = 0$, where m is the quantum number associated with the z component of the angular momentum $\hat{L}_z$. In this case we can take advantage of the cylindrical symmetry of the problem, and the term $\frac{1}{\rho^2}\frac{\partial^2}{\partial\phi^2}$ disappears. The interaction potential that describes the coupling of the laser field and the electron reads

$$\hat{V}_L(t) = \left(1 + \frac{1}{2M_p + 1}\right) zE(t). \tag{4}$$

The $\hat{L}_z$ operator commutes both with $\hat{H}_0$ and with $\hat{V}_L(t)$, so m is a constant of motion. The H_2^+ molecule has an inversion center, and since our initial wave function (the molecular ground state) is of g symmetry and the laser field is polarized along the internuclear axis, the absorption of an odd number of photons by the molecule will change its symmetry to u. On the other hand, the absorption of an even number of photons will not change the symmetry of the wave function. If we expanded the wave function on the basis of spherical harmonics $Y_l^{m=0}$, the absorption of an odd number of photons would lead to a combination of spherical harmonics with odd l, and in the same way the absorption of an even number of photons would lead to a combination of spherical harmonics with even l.

The external laser field is described by $E(t) = f(t)\sin(\omega t)$, where ω is the central frequency and the envelope function is defined as

$$f(t) = \begin{cases} E_0 \cos^2\left(\frac{\pi t}{T}\right) & |t| \leqslant \frac{T}{2}, \\ 0 & |t| > \frac{T}{2}, \end{cases} \tag{5}$$

where T is the total duration of the pulse and the peak intensity is defined as $I_0 = cE_0^2/(8\pi)$.

For the system described above, the 3D TDSE can be written as

$$\left(\hat{H}_0 + \hat{V}_L(t) - i\frac{\partial}{\partial t}\right)\Psi(R,\rho,z,t) = 0. \tag{6}$$

We discretize our wave function on a numerical lattice. To avoid the Coulomb singularity in the molecular potential at the nucleus we locate the first-lattice point in the ρ direction at $1/2$ of the grid spacing. In this way, the molecular potential will always be finite in our grid. A nonequidistant cubic grid is implemented for the description of the wave function near the nuclei, thus reducing the computational cost without sacrificing the accuracy of the description of the bound states. When using a nonequidistant grid, the resulting Hamiltonian matrix is non-Hermitian. To avoid this problem we multiply our wave function by the element of volume $\sqrt{\rho d\rho dz dR}$, so that the transformed Hamiltonian matrix becomes Hermitian [31,32]. The initial wave function (at $t = -T/2$) is the ground state of the system and is obtained by diagonalizing the unperturbed Hamiltonian using the routines that are available in SLEPC [33].

For the time propagation, we solve the TDSE by using the Crank-Nicolson propagator with a split-operator method that reduces the computational effort to the solution of a linear system of equations with a tridiagonal matrix

$$\begin{aligned}\Psi(R,\rho,z,t+\Delta t) = {} & e^{-iV\Delta t/2}e^{-i\hat{T}_R\Delta t}e^{-i\hat{T}_\rho\Delta t} \\ & \times e^{-i\hat{T}_z\Delta t}e^{-iV\Delta t/2}\Psi(R,\rho,z,t\Delta t) \\ & + O(\Delta t^3),\end{aligned} \tag{7}$$

where $V = V_C + V_L(t)$. We have used a numerical box with $|z| < 100$ a.u., $\rho < 50$ a.u., and $R < 30$ a.u. with grid spacings of $\Delta z = 0.1$ a.u., $\Delta\rho = 0.075$ a.u., and $\Delta R = 0.05$ a.u. at the center of the grid. These grid spacings gradually increase as we go to the limits of the box. For the electronic propagation, we use a time step $\Delta t_{\rm elec} = 0.011$ a.u., and for the nuclear propagation, we use a time step 10 times larger in order to save computational effort ($\Delta t_{\rm nuc} = 0.11$ a.u.). We have checked the convergence of the results with these parameters.

B. Molecular resolvent operator

The molecular-resolvent-operator method was introduced in [28,29]. Here we will briefly review this method and explain how angular distributions can be extracted.

Let Ψ be the molecular state that we want to analyze. Usually, Ψ is the state after the end of the pulse, obtained by solving the TDSE. At sufficiently long times, i.e., when the two protons are far away from each other, the BO approximation becomes exact, so that the resolvent operator can be factorized onto an electronic part and a nuclear part [28,29], namely,

$$\begin{aligned}\hat{R} = {} & \frac{\delta_N^{n_N}}{[(\hat{T}_N + E_k(R) + \varepsilon_e) - E_N - E_k(\infty) - \varepsilon_e]^{n_N} - i\delta_N^{n_N}} \\ & \times \frac{\delta_e^{n_e}}{[\hat{H}_{el} - E_k(R) - \varepsilon_e]^{n_e} - i\delta_e^{n_e}} \qquad (8) \\ \equiv {} & \hat{R}_N\hat{R}_{el}, \qquad (9)\end{aligned}$$

which is a direct product of two resolvent operators associated with the electronic energy ε_e and nuclear energy E_N supported by the electronic potential curve $E_k(R)$. Here n_i and δ_i ($i = e,N$) describe the order of the resolvent operator and the energy resolution for the different fragments, respectively. If $E_k(R)$ refers to a bound potential-energy curve, then ε_e is set to zero, while for a continuum state, ε_e refers to the electron energy in the continuum and $E_k = 1/R$. In the case of dissociative ionization of H_2^+, $E_k(\infty) = 0$. Therefore, by applying $\hat{R}$ to Ψ, one actually selects the kth molecular state in which the energy of the ejected electron is ε_e and the nuclear energy is E_N.

To obtain the electron angular distribution, we apply to $\hat{R}\Psi$ a projection operator that selects a small interval of electron emission angles around a given angle θ [26,27]. This projection operator is defined as

$$\hat{P}_{[\theta-\Delta\theta/2,\theta+\Delta\theta/2]}\Psi(z,\rho,R) = \begin{cases}\Psi(z,\rho,R) & \text{for } \theta - \Delta\theta/2 \leqslant \arctan(\rho/z) \leqslant \theta + \Delta\theta/2, \\ 0 & \text{otherwise.}\end{cases} \tag{10}$$

This procedure allows us to obtain a spectrum fully differential in both the energies of the fragments and the electron emission angle:

$$\frac{d^3P}{dE_N d\varepsilon_e d\theta} = \lim_{\Delta\theta\to 0}\frac{\langle\Psi|\hat{R}^\dagger\hat{P}_{[\theta-\Delta\theta/2,\theta+\Delta\theta/2]}\hat{R}|\Psi\rangle}{\Delta\theta\delta_e\pi\csc\left(\frac{\pi}{2n_e}\right)\delta_N\pi\csc\left(\frac{\pi}{2n_N}\right)}, \tag{11}$$

where the properties of the projection operator, $\hat{P}^\dagger = \hat{P} = \hat{P}^2$, have been used. By integrating this observable over different variables, one obtains the CKE and $\mathrm{CAK_N}$ spectra, respectively,

$$\frac{d^2P}{dE_N d\varepsilon_e} = \int d\theta\,\frac{d^3P}{dE_N d\varepsilon_e d\theta}, \tag{12}$$

$$\frac{d^2P}{dE_N d\theta} = \int d\varepsilon_e\,\frac{d^3P}{dE_N d\varepsilon_e d\theta}. \tag{13}$$

We have performed the ROM analysis by using the values $n_e = n_N = 2$, $\delta_e = 0.02$ and $\delta_N = 0.01$. For the angular resolution we have used $\Delta\theta = 4^\circ$. The ROM analysis is performed at the end of the pulse. We have checked the convergence of the results by propagating 1 fs after the end of the pulse. The results remain practically unchanged.

The ROM analysis was implemented and parallelized using PETSC routines [34]. A direct LU factorization solver (MUMPS) [35] was used to solve the electronic resolvent equations, and a Krylov solver was used for the nuclear resolvent equations. For a single ROM analysis of the final wave function, the computations required 3 days on 64 processors and 50 GB of memory. The ROM analysis is more demanding than the propagation of the TDSE.

III. RESULTS

In this section we present the calculated KER, CKE, and CAK_N spectra for dissociative ionization of H_2^+. We have used relatively low intensities (10^{12} W/cm^2) and pulses with central frequency $\omega = 0.4$, 0.6, and 0.8 a.u. For this choice of the laser parameters, the Keldysh parameter [36] is much larger than 1 ($\gamma \gg 1$), so that we are in the multiphoton ionization regime. Although we are working with relatively low intensities, a perturbative approach may be not valid since in some cases there are intermediate N-photon resonances within the Franck-Condon region. For example, for $\omega = 0.4$ a.u., there is a one-photon resonant transition from the $1s\sigma_g$ to the $2p\sigma_u$ electronic state, so a nonperturbative approach must be used. To investigate the effect of pulse duration on the spectra, we have considered $T = 0.76$, 1.14, and 2.5 fs for $\omega = 0.8$ a.u. and $T = 0.5$, 1.0 and 2.5 fs for $\omega = 0.4$ and 0.6 a.u.

A. Born-Oppenheimer curves

We first discuss the specificities of the multiphoton ionization process by looking at the Born-Oppenheimer diagrams given in Fig. 2. For the three central frequencies considered in Figs. 2(a), 2(b), and 2(c), one can expect that, in the monochromatic (long pulse duration) limit, one-photon ionization is a forbidden process since the photon energy is smaller than the vertical ionization potential. In this limit, two-photon ionization is expected to be the dominant channel for $\omega = 0.8$ and 0.6 a.u., and three-photon ionization is expected to be dominant for $\omega = 0.4$ a.u.

This picture changes when sub-fs pulses are used because, due to the large bandwidth of these pulses, new ionization channels can be opened. Indeed, Fig. 2 shows that the bandwidth of the shortest pulses are of the order of the central frequency of the corresponding pulse ω. Thus, for $\omega = 0.8$ a.u. [Fig. 2(a)] and a duration $T = 0.76$ fs, the one-photon absorption channel is also open in the Franck-Condon region since the electronic continuum can be reached in a vertical transition from the ground state by absorption of a photon lying in the large-R region of the Franck-Condon zone. Similarly, for $\omega = 0.4$ a.u. [Fig. 2(c)] and a duration $T = 0.5$ fs, two-photon absorption is also possible. As the probability of absorbing $N-1$ photons is much higher than that of absorbing N photons (in perturbation theory), one can expect that the $(N-1)$-photon ionization channel will be comparable to or even dominate over the N-photon ionization channel.

B. Kinetic-energy-release spectra

In Fig. 3, we show the KER spectra for all the cases considered in this work. According to the Franck-Condon principle, we expect that, in all cases, the spectra will be centered at $E_N \approx 1/R_{eq} \approx 0.5$ a.u., which is the value of the repulsive Coulomb potential-energy curve associated with the ionization limit at the equilibrium internuclear distance R_{eq}. However, if one examines the results more closely, deviations from the expected results can be noticed.

In Fig. 3(b), for $\omega = 0.6$ a.u., we compare our results with those available in the literature [23]. The agreement is good. In this case, two-photon ionization is the dominant process for

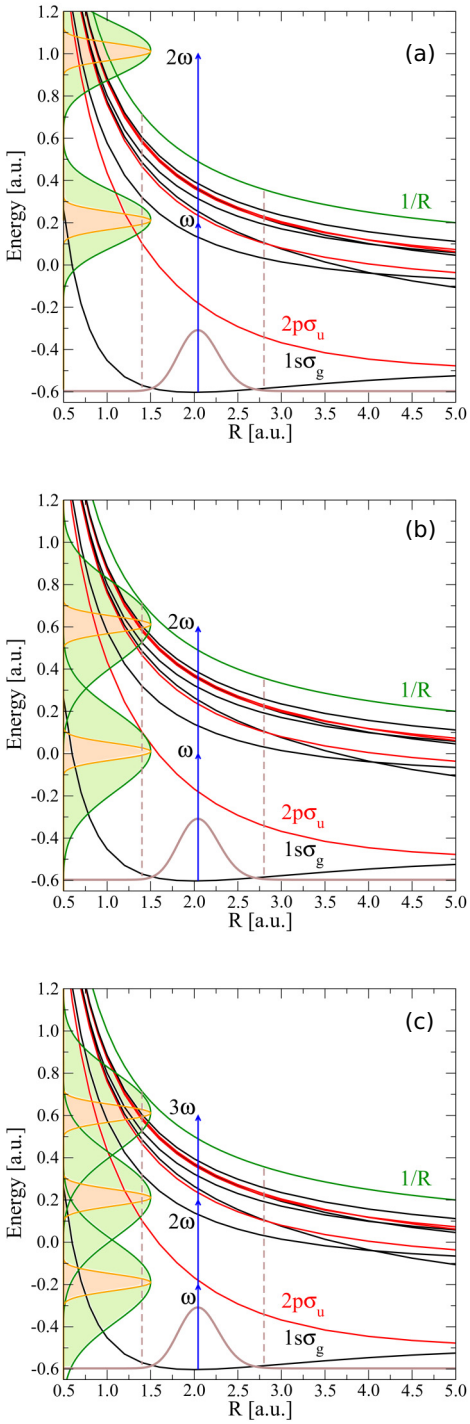

FIG. 2. (Color online) Born-Oppenheimer potential-energy curves for the H_2^+ molecule. The black curves correspond to states of σ_g symmetry, and the red ones show those of σ_u symmetry. The blue arrows represent a vertical transition from the ground state to the ionization continuum. (a) shows arrows corresponding to the photon energy $\omega = 0.8$ a.u. and the Fourier transforms of pulses with durations $T = 2.5$ fs and $T = 0.76$ fs, in green and orange, respectively, shifted by the energy of the photon. (b) and (c) are similar to (a) but are for a photon energy $\omega = 0.6$ a.u. and $\omega = 0.4$ a.u., respectively. In this case, the Fourier transform corresponds to pulses of duration $T = 2.5$ fs and $T = 0.5$ fs. The Franck-Condon region lies in between the vertical dashed lines.

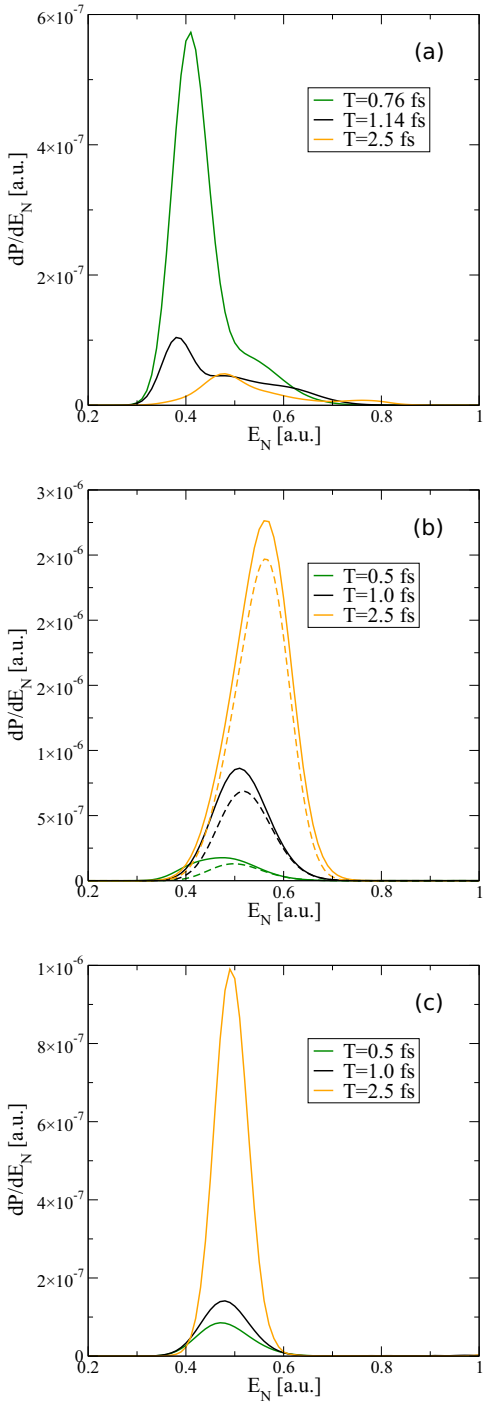

FIG. 3. (Color online) KER spectra resulting from pulses with central frequencies (a) $\omega = 0.8$ a.u., (b) $\omega = 0.6$ a.u., and (c) $\omega = 0.4$ a.u. The pulse duration is indicated in each panel. In (b) we also show the results from Ref. [23] (dashed lines).

the three pulse durations considered in our calculations. For the shorter pulse, $T = 0.5$ fs, the distribution is very similar to that resulting from the Franck-Condon overlaps between the initial vibrational state and the final dissociative states (see [23]), which proves that, for such a short pulse duration, two-photon absorption is a near-vertical transition. One can see, however, that, as pulse duration increases, the maximum of the ionization probability shifts to higher nuclear energies, thus departing from the Franck-Condon behavior. This is a consequence of the variation of the one- and two-photon dipole transition amplitudes with internuclear distance and the fact that, as pulse duration increases, a resonant one-photon transition populates the $2p\sigma_u$ state at smaller R, thus generating a nuclear wave packet that can significantly move before the second photon is absorbed. The combination of these effects destroys the picture of a vertical two-photon vertical transition from the ground state. Similar effects explain the shift in the probability maximum for $\omega = 0.4$ a.u. [see Fig. 3(c)].

The case shown in Fig. 3(a) for $\omega = 0.8$ a.u. is more interesting. First, we notice that the total probability is larger for the shorter than for the longer pulses, in contrast to the behavior observed in the two cases discussed in the previous paragraph. The reason for this behavior is that, for durations $T = 0.76$ fs and $T = 1.14$ fs, the one-photon ionization channel is open, and the corresponding ionization probability is much larger than that of the two-photon ionization channel. For the longest pulse duration, $T = 2.5$ fs, the one-photon ionization channel is closed, so that the total ionization yield follows a pattern closer to that discussed for $\omega = 0.6$ a.u. For the shortest pulse ($T = 0.76$ fs), the signature of the one-photon ionization process is the maximum at $E_N \approx 0.4$ a.u., while that of the two-photon ionization process is the shoulder at $E_N \approx 0.5$ a.u. The lower value of E_N in the former case is due to the fact that, for this pulse duration, reaching the ionization continuum by absorption of a single photon is possible only at the larger values of R within the Franck-Condon region. This is the only region where the ionization potential is smaller than the energy of the higher spectral components of the pulse [see Fig. 2(a)]. For the intermediate pulse duration ($T = 1.14$ fs), one- and two-photon ionization processes cannot be so easily identified. In this case, as we will see later, the analysis of the CKE and $\mathrm{CAK_N}$ spectra will provide a much more complete picture.

C. Correlated spectra

In this section, we present our results for the CKE and the $\mathrm{CAK_N}$ spectra, which provide a more detailed information of the ionization process.

1. Correlated kinetic-energy spectra

We show in Fig. 4 the calculated CKE spectra for all the cases under study. Note that in the monochromatic limit (infinite pulse duration) we expect to see energy conservation lines [28,29,37,38] satisfying the relationship $N\omega = E_e + E_N + D_{2H^+}$, where $D_{2H^+} = -E_0 = 0.597$ a.u. is the threshold energy required to produce two protons at infinite internuclear distance, E_0 is the ground-state energy, E_e and E_N are the electronic and nuclear energies, respectively, and N is the number of absorbed photons. The expected energy-conservation lines are shown as dashed magenta lines in Fig. 4.

For the longest pulse, $T = 2.5$ fs, with central frequencies $\omega = 0.8$ and 0.6 a.u., one can clearly observe a strong signal along the energy-conservation line for $N = 2$ [right panels in Figs. 4(a) and 4(b)]. For $\omega = 0.4$ a.u. [right panel in Fig. 4(c)],

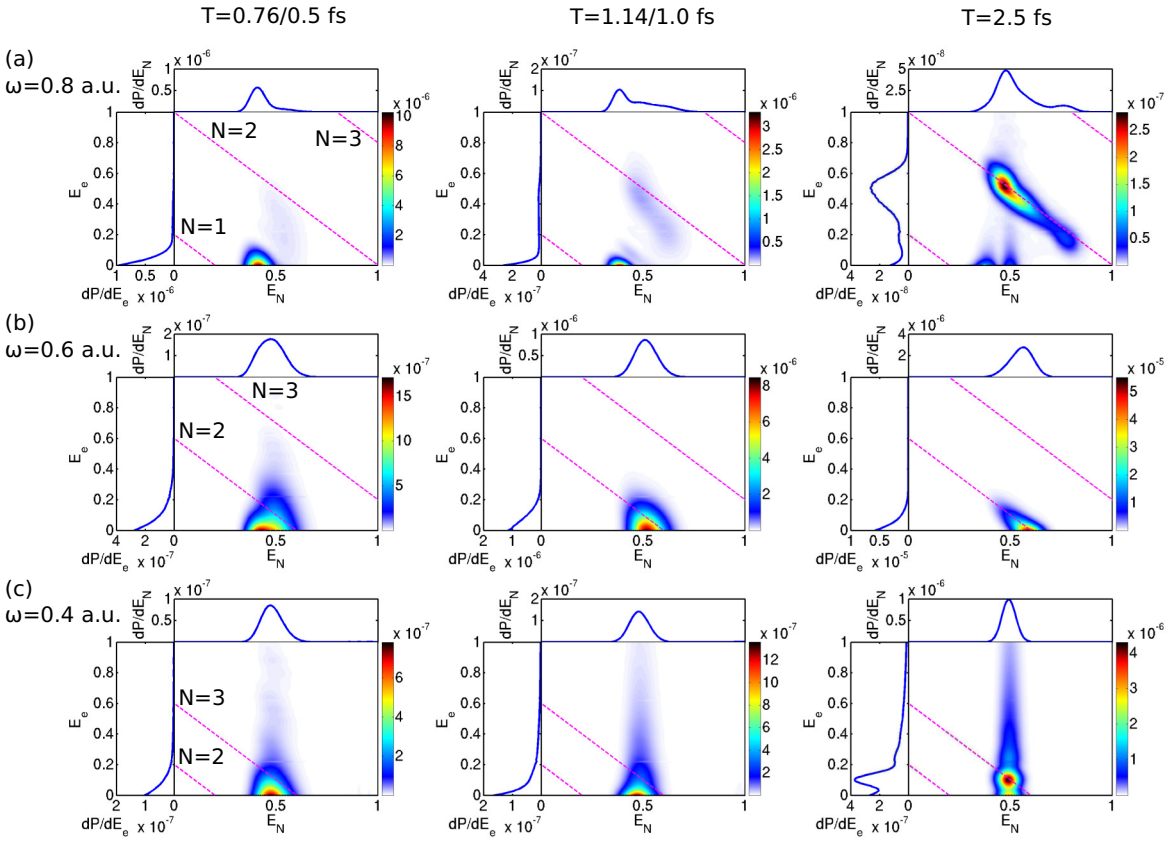

FIG. 4. (Color online) CKE for different pulses. The projections (singly differential probabilities) are shown at the left and at the top of each CKE spectrum. (a) Central frequency $\omega = 0.8$ a.u. and pulse durations $T = 0.76$, 1.14, and 2.5 fs (left, middle, and right panels, respectively). (b) and (c) Central frequencies $\omega = 0.6$ a.u. and $\omega = 0.4$ a.u., respectively, and pulse durations $T = 0.5$, 1.0, and 2.5 fs (left, middle, and right panels, respectively). Energy-conservation lines for absorption of N photons are indicated by dashed magenta lines. All the results and scales are in atomic units.

the bright spot in the spectrum at $(E_N, E_e) \approx (0.5, 0.1)$ a.u. is explained by the same energy-conservation law with $N = 3$. In contrast, for the other pulse durations, it is harder to see a clear signature of energy-conservation lines. In particular, for a central frequency $\omega = 0.4$ a.u. and pulse durations $T = 0.5$ fs and $T = 1.0$ fs, the bright spot appearing at $E_N \approx 0.5$ a.u. is no longer present at the expected location, which is an indication of a two-photon process rather than a three-photon one. Also, for a central frequency $\omega = 0.8$ a.u. [Fig. 4(a)], one can clearly observe the transition from two-photon ionization to one-photon ionization as the pulse duration decreases, and for $\omega = 0.6$ a.u. [Fig. 4(b)], one can see the shift of the maximum to lower nuclear energy (see discussion in the previous section). Indeed, the region of low electron energies dominates the spectrum for $T = 0.76$ fs and $T = 1.14$ fs, which is an indication of one-photon ionization. For the longest pulse duration, however, the one-photon ionization channel is closed, and the ionization threshold can only be reached by absorption of two photons.

2. *Correlated angular and nuclear kinetic-energy spectra*

Figure 5 shows the $\mathrm{CAK_N}$ spectra. To interpret these results, one must take into account the fact that absorption of an odd (even) number of photons results in a combination of partial waves involving spherical harmonics $Y_l^{m=0} \propto P_l^{m=0}(\cos\theta)$ with odd (even) l. Thus, one can expect that the nodal structure of the corresponding Legendre polynomials will be imprinted in the $\mathrm{CAK_N}$ spectra. Although l is not a good quantum number for $H_2{}^+$ and therefore the photoionization selection rules are not the same as for atomic systems, one can still see reminiscences of the latter in the $\mathrm{CAK_N}$ spectra because the ground state of $H_2{}^+$ has a predominant $l = 0$ character.

Figure 5(b) ($\omega = 0.6$ a.u.) shows that, for the pulse durations $T = 1.0$ fs and $T = 2.5$ fs, the $\mathrm{CAK_N}$ spectra exhibit nodes at $\cos\theta \approx \pm 0.5$, which is the signature of a d wave (the nodes of the $P_2^{m=0}$ Legendre polynomial strictly appear at $\cos\theta = \pm 0.57735$). For the shortest pulse ($T = 0.5$ fs), the angular distribution is not symmetric due to the fact that, for such a short duration, the effect of the carrier-envelope phase (CEP) is not negligible. In any case, the presence of the two nodes at $\cos\theta \approx \pm 0.5$ confirms that the spectra for a central frequency $\omega = 0.6$ a.u. are almost entirely due to a two-photon transition.

In Fig. 5(c) ($\omega = 0.4$ a.u.), the $\mathrm{CAK_N}$ spectra look quite different depending on the pulse duration. For the shortest pulses, the angular distributions resemble those in Fig. 5(b) (signature of the d wave). As discussed above, this is due to the fact that, as a result of the large bandwidth, two-photon ionization is possible and is the dominant process (see Fig. 2). We were already driven to this conclusion,

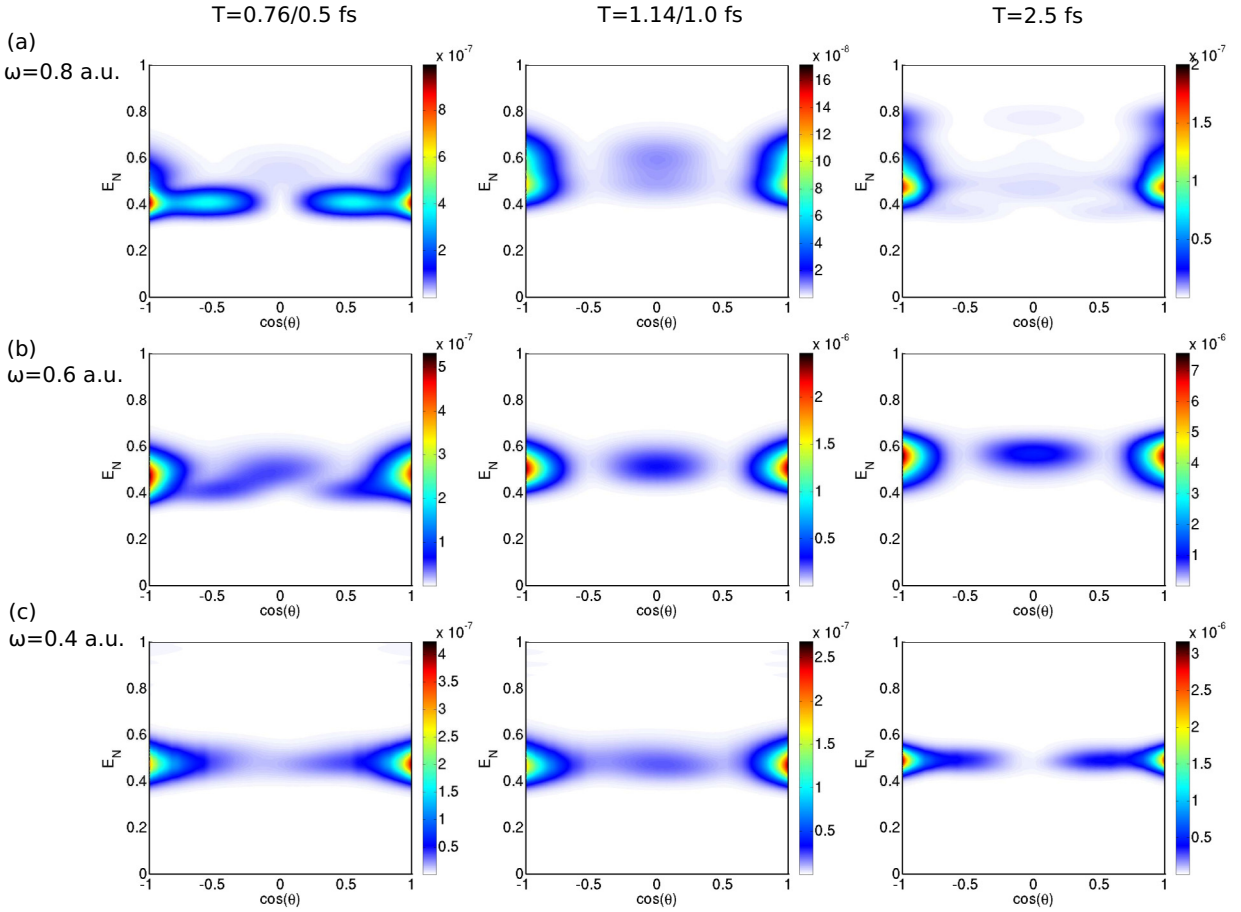

FIG. 5. (Color online) Same as in Fig. 4, but for the CAK_N spectra. All the results and scales are in atomic units.

although less clearly, by looking at the corresponding CKE spectra. However, such information could not be inferred at all by looking at the KER spectra. By increasing the pulse duration while keeping constant the central frequency [Fig. 5(c), right], we observe a nodal plane at $\cos\theta = 0$ and a little bump at $\cos\theta \approx 0.75$, which is the signature of an f wave, thus indicating that absorption of an odd number of photons has occurred. Since one-photon ionization at these low frequencies is very unlikely [see Fig. 2(c)], we thus conclude that the spectra are dominated by three-photon ionization.

In Fig. 5(a) ($\omega = 0.8$ a.u.), one can also see a clear variation of the spectra with the pulse duration. We already know, from the analysis of the CKE spectra presented above, that as the pulse duration decreases, one passes from a dominant two-photon ionization regime to a different one in which the contribution from one-photon ionization becomes progressively more important. The CAK_N spectra show this effect even more clearly. Indeed, Fig. 5(a) (left) shows the appearance of a nodal plane at $\cos\theta = 0$, thus indicating that absorption of one photon is the dominant process. As one moves from the left to the right panels in Fig. 5(a), i.e., as the pulse duration increases, one can see that the nodal plane at $\cos\theta = 0$ disappears and the overall shape of the spectrum becomes closer to that found for $\omega = 0.6$ a.u. [Fig. 5(b)]. In fact, for $T = 1.0$ fs and $T = 2.5$ fs, the CAK_N spectra reflect contributions from both processes. To better visualize these contributions, we have performed a separate ROM analysis for the g and u symmetry components of the wave function. The results are shown in Fig. 6. One can clearly see that one-photon ionization, which, as explained above, leads to lower nuclear kinetic energies, appears in the u part of the spectrum, where a node at $\cos\theta = 0$ is clearly visible. In contrast, two-photon ionization, which shows up at slightly higher nuclear kinetic energies, appears in the g part of the spectrum, where the nodes at $\cos\theta \approx \pm 0.5$ are apparent.

IV. CONCLUSIONS

We have presented an extension of the resolvent operator method to extract fully differential ionization probabilities in H_2^+ by including all electronic and vibrational (dissociative) degrees of freedom. We have focused on multiphoton dissociative ionization induced by moderately intense laser fields. The wave function from which ionization probabilities are extracted has been obtained by solving the TDSE for the case of the H_2^+ molecule oriented parallel to the polarization direction of the field. When possible, our results have been successfully compared with those previously obtained in the literature [23].

The CKE and CAK_N spectra have been evaluated and used to analyze the underlying mechanisms of the photoionization process. In particular, for pulses with a central energy

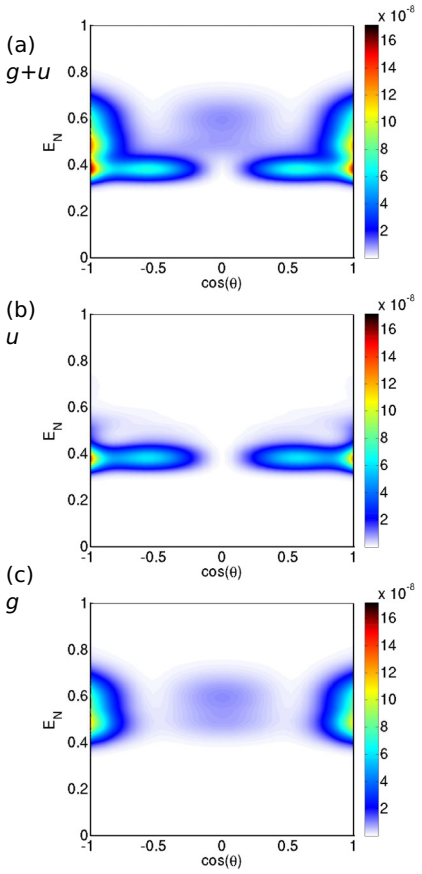

FIG. 6. (Color online) Contributions to the CKA_N spectrum from different molecular symmetries for a pulse with central frequency $\omega = 0.8$ a.u. and duration $T = 1.14$ fs. (a) The total CAK_N spectrum and the (b) u and (c) g contributions. All the results and scales are in atomic units.

$\hbar\omega = 0.8$ a.u., which is smaller than the vertical ionization potential of H_2^+ at the internuclear equilibrium distance, we have shown the opening of the one-photon ionization channel by decreasing the pulse duration down to the sub-fs time scale. This effect, namely, the opening of the $(N-1)$-photon ionization channel when the central energy is such that ionization requires N such photons, is expected to occur for any pulse of sufficiently short duration. Our results for a central frequency $\omega = 0.4$ a.u. confirm this expectation. An inspection of the CKE and CAK_N spectra clearly shows the variation of the relative contribution of $(N-1)$- and N-photon ionization processes with pulse duration. The latter information is difficult to obtain when only the KER spectrum is measured. This points out the importance of performing multiple-coincidence measurements for better elucidation of competing ionization mechanisms, such as those arising when ultrashort pulses are used.

ACKNOWLEDGMENTS

We gratefully acknowledge fruitful discussions with Dr. A. Palacios. This work was accomplished with an allocation of computer time from Mare Nostrum BSC and CCC-UAM and was partially supported by European Research Council Advanced Grant No. XCHEM 290853, MINECO Project No. FIS2013-42002-R, ERA-Chemistry Project No. PIM2010EEC-00751, European Grant No. MC-ITN CORINF, European COST Action XLIC CM1204, and the CAM project NANOFRONTMAG. H.B. acknowledges support for mobility from ITN CORINF and is grateful for the hospitality of the Universidad Autónoma de Madrid. R.E.F.S. acknowledges FCT - Fundação para a Ciência e Tecnologia, Portugal, Grant No. SFRH/BD/84053/2012.

[1] T. Shintake, H. Tanaka, T. Hara, T. Tanaka, K. Togawa, M. Yabashi, Y. Otake, Y. Asano, T. Bizen, T. Fukui *et al.*, Nat. Photonics **2**, 555 (2008).

[2] W. Ackermann, G. Asova, V. Ayvazyan, A. Azima, N. Baboi, J. Bähr, V. Balandin, B. Beutner, A. Brandt, A. Bolzmann *et al.*, Nat. Photonics **1**, 336 (2007).

[3] J. J. Macklin, J. D. Kmetec, and C. L. Gordon, Phys. Rev. Lett. **70**, 766 (1993).

[4] A. L'Huillier and P. Balcou, Phys. Rev. Lett. **70**, 774 (1993).

[5] M. Hentschel, R. Kienberger, C. Spielmann, G. A. Reider, N. Milosevic, T. Brabec, P. Corkum, U. Heinzmann, M. Drescher, and F. Krausz, Nature (London) **414**, 509 (2001).

[6] M. Schultze, M. Fieß, N. Karpowicz, J. Gagnon, M. Korbman, M. Hofstetter, S. Neppl, A. L. Cavalieri, Y. Komninos, T. Mercouris *et al.*, Science **328**, 1658 (2010).

[7] K. Klünder, J. M. Dahlström, M. Gisselbrecht, T. Fordell, M. Swoboda, D. Guénot, P. Johnsson, J. Caillat, J. Mauritsson, A. Maquet *et al.*, Phys. Rev. Lett. **106**, 143002 (2011).

[8] P. Eckle, A. Pfeiffer, C. Cirelli, A. Staudte, R. Dörner, H. Muller, M. Büttiker, and U. Keller, Science **322**, 1525 (2008).

[9] F. Kelkensberg, C. Lefebvre, W. Siu, O. Ghafur, T. T. Nguyen-Dang, O. Atabek, A. Keller, V. Serov, P. Johnsson, M. Swoboda *et al.*, Phys. Rev. Lett. **103**, 123005 (2009).

[10] G. Sansone, F. Kelkensberg, J. Pérez-Torres, F. Morales, M. F. Kling, W. Siu, O. Ghafur, P. Johnsson, M. Swoboda, E. Benedetti *et al.*, Nature (London) **465**, 763 (2010).

[11] P. Ranitovic, C. W. Hogle, P. Rivière, A. Palacios, X.-M. Tong, N. Toshima, A. González-Castrillo, L. Martin, F. Martín, M. M. Murnane *et al.*, Proc. Natl. Acad. Sci. **111**, 912 (2014).

[12] M. Kling, C. Siedschlag, A. J. Verhoef, J. Khan, M. Schultze, T. Uphues, Y. Ni, M. Uiberacker, M. Drescher, F. Krausz *et al.*, Science **312**, 246 (2006).

[13] F. Calegari, D. Ayuso, A. Trabattoni, L. Belshaw, S. De Camillis, S. Anumula, F. Frassetto, L. Poletto, A. Palacios, P. Decleva *et al.*, Science **346**, 336 (2014).

[14] P. Tzallas, E. Skantzakis, L. Nikolopoulos, G. D. Tsakiris, and D. Charalambidis, Nat. Phys. **7**, 781 (2011).

[15] P. A. Carpeggiani, P. Tzallas, A. Palacios, D. Gray, F. Martín, and D. Charalambidis, Phys. Rev. A **89**, 023420 (2014).

[16] Y. H. Jiang, A. Rudenko, J. F. Pérez-Torres, O. Herrwerth, L. Foucar, M. Kurka, K. U. Kühnel, M. Toppin, E. Plésiat, F. Morales *et al.*, Phys. Rev. A **81**, 051402 (2010).

[17] Y. H. Jiang, A. Rudenko, E. Plésiat, L. Foucar, M. Kurka, K. U. Kühnel, T. Ergler, J. F. Pérez-Torres, F. Martín, O. Herrwerth *et al.*, Phys. Rev. A **81**, 021401 (2010).
[18] A. Palacios, A. González-Castrillo, and F. Martín, Proc. Natl. Acad. Sci. **111**, 3973 (2014).
[19] R. Dörner, V. Mergel, O. Jagutzki, L. Spielberger, J. Ullrich, R. Moshammer, and H. Schmidt-Böcking, Phys. Rep. **330**, 95 (2000).
[20] M. Odenweller, J. Lower, K. Pahl, M. Schütt, J. Wu, K. Cole, A. Vredenborg, L. P. Schmidt, N. Neumann, J. Titze *et al.*, Phys. Rev. A **89**, 013424 (2014).
[21] S. Barmaki, H. Bachau, and M. Ghalim, Phys. Rev. A **69**, 043403 (2004).
[22] A. Palacios, H. Bachau, and F. Martín, J. Phys. B **38**, L99 (2005).
[23] A. Palacios, S. Barmaki, H. Bachau, and F. Martín, Phys. Rev. A **71**, 063405 (2005).
[24] J. L. Sanz-Vicario, H. Bachau, and F. Martín, Phys. Rev. A **73**, 033410 (2006).
[25] J. Javanainen, J. H. Eberly, and Q. Su, Phys. Rev. A **38**, 3430 (1988).
[26] K. J. Schafer and K. C. Kulander, Phys. Rev. A **42**, 5794 (1990).
[27] F. Catoire and H. Bachau, Phys. Rev. A **85**, 023422 (2012).
[28] R. E. F. Silva, F. Catoire, P. Rivière, H. Bachau, and F. Martín, Phys. Rev. Lett. **110**, 113001 (2013).
[29] F. Catoire, R. E. F. Silva, P. Rivière, H. Bachau, and F. Martín, Phys. Rev. A **89**, 023415 (2014).
[30] J. R. Hiskes, Phys. Rev. **122**, 1207 (1961).
[31] T. Niederhausen, U. Thumm, and F. Martín, J. Phys. B **45**, 105602 (2012).
[32] M. W. J. Bromley and B. D. Esry, Phys. Rev. A **69**, 053620 (2004).
[33] C. Campos, J. E. Román, E. Romero, A. Tomás, V. Hernández, and V. Vidal, SLEPC users manual, http://www.grycap.upv.es/slepc/.
[34] S. Balay, S. Abhyankar, M. F. Adams, J. Brown, P. Brune, K. Buschelman, L. Dalcin, V. Eijkhout, W. D. Gropp, D. Kaushik *et al.*, Argonne National Laboratory, Technical Report ANL-95/11, revision 3.5, 2014 (unpublished), http://www.mcs.anl.gov/petsc.
[35] P. R. Amestoy, I. S. Duff, J.-Y. L'Excellent, and J. Koster, SIAM J. Matrix Anal. Appl. **23**, 15 (2001).
[36] L. V. Keldysh, Sov. Phys. JETP **20**, 1018 (1965).
[37] C. B. Madsen, F. Anis, L. B. Madsen, and B. D. Esry, Phys. Rev. Lett. **109**, 163003 (2012).
[38] J. Wu, M. Kunitski, M. Pitzer, F. Trinter, L. P. H. Schmidt, T. Jahnke, M. Magrakvelidze, C. B. Madsen, L. B. Madsen, U. Thumm *et al.*, Phys. Rev. Lett. **111**, 023002 (2013).